Statistical mechanics of shell models for two-dimensional turbulence

E. Aurell
Department of Mathematics, Stockholm University, S-106 91 Stockholm, Sweden

G. Boffetta
Istituto di Fisica Generale, Università di Torino, Via Pietro Giuria 1, I-10125 Torino, Italy

A. Crisanti
Dipartimento di Fisica, Università di Roma "La Sapienza," Piazzale Aldo Moro 2, I-00185 Roma, Italy

P. Frick
Institute of Continuous Media Mechanics, Russian Academy of Sciences, 1, Acad. Korolyov Str., 614061, Perm, Russia

G. Paladin
Dipartimento di Fisica, Università dell'Aquila Via Vetoio, Coppito I-67100 L'Aquila, Italy

A. Vulpiani
Dipartimento di Fisica, Università di Roma "La Sapienza," Piazzale Aldo Moro 2, I-00185 Roma, Italy
(Received 9 May 1994)

We study shell models that conserve the analogs of energy and enstrophy, and hence are designed to mimic fluid turbulence in two dimensions (2D). The main result is that the observed state is well described as a formal statistical equilibrium, closely analogous to the approach to two-dimensional ideal hydrodynamics of Onsager [Nuovo Cimento Suppl. **6**, 279 (1949)], Hopf [J. Rat. Mech. Anal. **1**, 87 (1952)], and Lee [Q. Appl. Math. **10**, 69 (1952)]. In the presence of forcing and dissipation we observe a forward flux of enstrophy and a backward flux of energy. These fluxes can be understood as mean diffusive drifts from a source to two sinks in a system which is close to local equilibrium with Lagrange multipliers ("shell temperatures") changing slowly with scale. This is clear evidence that the simplest shell models are not adequate to reproduce the main features of two-dimensional turbulence. The dimensional predictions on the power spectra from a supposed forward cascade of enstrophy and from one branch of the formal statistical equilibrium coincide in these shell models in contrast to the corresponding predictions for the Navier-Stokes and Euler equations in 2D. This coincidence has previously led to the mistaken conclusion that shell models exhibit a forward cascade of enstrophy. We also study the dynamical properties of the models and the growth of perturbations.

PACS number(s): 47.27.Gs, 47.27.Eq

I. INTRODUCTION

The idea of shell models of turbulence [1–7] is to replace the fluctuations of a turbulent field in an octave of wave numbers $2^n < |k| < 2^{n+1}$ by one or a few representative variables. The range of wave numbers is called a shell and the variables are called shell variables. The dynamics of the shell variables should be chosen so as to preserve as many as possible of the qualitative features of the full equations. In this way, it is possible to describe the cascade processes of inertially conserved quantities by a chaotic dynamical system with a limited number of degrees of freedom. Predictions from dimensional analysis can then be tested with far greater accuracy than in full simulations of the Navier-Stokes equations.

This approach has been particularly successful for three-dimensional (3D) turbulence in the models introduced by Gledzer [8] and Yamada and Ohkitani [5] (see also [6] or [9]), which, following the recent literature, we will refer to as the GOY models. Nevertheless it has recently become clear that the situation is more complicated. Particular variants of the GOY models have in fact stable fixed points, corresponding to the Kolmogorov scaling law in 3D [10]. The dimensional predictions for the energy spectra come out correctly in these models [10], but there are no intermittency corrections and the whole phenomenology of a turbulent state (e.g., sensitivity to initial conditions and positive Lyapunov exponents) is absent.

We will report here on another instance where shell models give significantly different results than expected at first: shell models designed to model fluid turbulence in 2D. We will show that these models are perfectly well described by a formal statistical mechanics, closely similar to the approach of Onsager [11], Hopf [12], and Lee [13] for inviscid 2D hydrodynamics (see also the review [14]). If energy and enstrophy are pumped into the system by an external force and removed by viscous terms, we do observe a net mean flux of both energy and enstrophy from the force to the viscous sinks. These fluxes are shown to be analogous to mean drifts proportional to the gradients of the conjugate quantities, as in a sys-

tem which is locally, but not globally, in thermodynamic equilibrium. There is no need to invoke a cascade either in the inverse direction (of energy) or in the forward direction (of enstrophy). We show that in these shell models the dimensional predictions on the energy spectrum from a supposed forward cascade of enstrophy coincide with equipartition of shell enstrophies, which is one of the branches of the statistical equilibrium. In previous investigations [15–17] the simpler explanation of the observed spectrum in terms of a weakly perturbed equlibria was overlooked.

The paper is organized as follows. In Sec. II we review the standard phenomenology of 2D turbulence and the minimal constraints which have to be put on shell models to take into account the difference to 3D. We present the shell models tested in the simulations, which are all extensions and variations of the 2D GOY model studied by several authors [8,15–17]. In Sec. III we recall the statistical equilibrium approach and apply it to determine the scaling laws and the probability distribution functions of the shell models. In Sec. IV we present numerical results on a steady forced state with enstrophy and energy output and compare them with the predictions of Sec. III. In Sec. V we present the results on dynamical properties, which are quite different from the results for 3D shell models, but consistent with what is expected from a system close to equilibrium. In Sec. VI we summarize our results.

II. 2D TURBULENCE AND SHELL MODELS

The main particularity of 2D Euler equations is that the vorticity is a material invariant, i.e., conserved along stream lines. This leads to an infinite number of additional integrals of motion since the global integral of any functional of vorticity is inertially preserved. In practice one habitually considers the lowest polynomial positive invariant, the enstrophy. One of the main reasons for this is that the enstrophy is also an invariant of the truncated Euler equations in Fourier space [14]. Although energy and enstrophy are both conserved globally, their support in wave vector space may change over time. The changes must be in opposite directions, such that if enstrophy is transported toward small scales (large wave numbers) energy is transported to large scales (small wave numbers).

The Navier-Stokes equations describe in addition to the inertial motion the action of external forcing and molecular viscosity. The first major difference to the situation in 3D is that in 2D molecular viscosity cannot remove energy efficiently because enstrophy contains two more derivatives, is dissipated first, and energy is then constrained to flow to large scales. This implies that in numerical investigations an infrared viscous term $-\nu'(-\Delta)^{-\gamma}$ is necessary to remove energy at large scales:

$$\partial_t \vec{u} + (\vec{u}\cdot\vec{\nabla})\vec{u} = -\vec{\nabla}P + \nu\Delta\vec{u} - \nu'(-\Delta)^{-\gamma}\vec{u} + \vec{F}\ , \quad (1)$$
$$\vec{\nabla}\cdot\vec{u} = 0\ , \qquad \vec{\nabla}\cdot\vec{F} = 0\ .$$

The exponent γ is rather arbitrary. For instance, γ in (1) equal to zero corresponds to linear friction, which describes the physical situation of a fluid flow in thin films with viscous drag in boundary layers. If one is mainly interested in the backward energy cascade ranges it is better to take a sharper artificial infrared viscosity, for which the action is more concentrated in a small range of wave numbers. This procedure is standard in numerical investigations of the 2D Navier-Stokes equations (see, e.g., [18,19,14]).

We will assume from now on that the force acts only on scales with typical wave number k_f and that the molecular and infrared viscosities act on scales much smaller and much larger, respectively. The spectrum can then be divided into five ranges: the energy dissipation range, where the infrared viscosity acts effectively; the inverse inertial transport range, where energy flows towards large scales; the scale of the forcing; the forward inertial transport range, where enstrophy flows towards small scales; and the enstrophy dissipation range, where molecular viscosity acts effectively.

The first attempts to predict the behavior of hydrodynamics in 2D used a formal statistical mechanics analogy for the Euler equations. We review this approach in Sec. III. A later approach due to Kraichnan and Batchelor proceeds along the lines of the Kolmogorov cascade picture for 3D [20]. For the forward transport range, a cascade of enstrophy implies by dimensional arguments that the energy spectrum should be $E(k) \sim k^{-3}$. Similarly, for the inverse transport range, an inverse cascade of energy gives $E(k) \sim k^{-\frac{5}{3}}$ [21,22,14].

In 3D there is strong experimental support of the cascade picture [23], albeit with intermittency corrections [24,25]. The evidence for cascade processes in 2D is not as clear. In the forward range, a energy spectrum steeper than k^{-3} implies that the most important interactions are not local in wave number space. A scaling k^{-3} is marginal and the dimensional predictions based on a cascade process with local interactions in k space are questionable. In fact, most numerical investigations of the 2D Navier-Stokes equations report spectra which are significantly steeper than k^{-3} [26,27]. However, all numerical investigations of the full Navier-Stokes equations suffer from a limited range of wave numbers for the inertial ranges. The k^{-3} energy spectrum cannot therefore be conclusively ruled out, while the prediction of the statistical equilibrium approach, which is k^{-1}, is clearly excluded by the numerical observations.

The true state of the 2D Navier-Stokes equations in the inverse cascade range is unclear. Most simulation have reported a $k^{-\frac{5}{3}}$ spectrum in agreement with the dimensional predictions [18,28]. The latest investigation over much longer time scales instead reports a k^{-3} spectrum extending to scales about one order of magnitude larger than the forcing and then a spectrum clearly much flatter than $k^{-\frac{5}{3}}$ [19]. In the inverse range the prediction from statistical equilibrium, which is $E(k) \sim k$, does not therefore seem to be completely ruled out.

The shell models we consider should be taken as the simplest systems that share the property of having two inertially conserved quadratic quantities. They are systems of coupled ordinary equations which may in general be written as

$$\frac{d}{dt}W_n = \sum_{m,l} X_{nml} W_m W_l - K_n W_n + F_n \ , \qquad (2)$$

where X indicates the nonlinear interactions, K the viscous forces, and F an external force. In (2) we have suppressed an index of shell variables within one shell. In the extreme case considered in the literature [7] this can be a moderately large number, of the order of 10^2. In the cases we consider, we will have one or a few complex shell variables per shell, with nonlinear terms that are compactly expressed using the complex conjugates W_n^*.

We use the convention that the shell variable W_n is like a shell vorticity, so (2) is a model of the vorticity equation. The quantities that should be inertially conserved are then "enstrophy"

$$\Omega = \sum_n |W_n|^2 \qquad (3)$$

and "energy"

$$E = \sum_n \left| \frac{1}{k_n} W_n \right|^2 , \qquad (4)$$

where k_n is the typical wave number of shell n. We will only consider the case where the k_n's are spaced in octaves, i.e., $k_n = k_0\, 2^n$.

The dimensional predictions are based on the assumption of cascade processes and from the observation that the fluxes of energy $\Pi_n(E)$ and of enstrophy $\Pi_n(\Omega)$ through the nth shell are given by certain third-order correlation functions [9]. For the 2D GOY model [see Eq. (12)] they read in detail

$$\Pi_n(\Omega) = \langle \mathrm{Re}(4W_n W_{n-1} W_{n-2} - W_{n+1} W_n W_{n-1}) \rangle \ , \qquad (5)$$

$$\Pi_n(E) = \frac{4}{k_n^2} \langle \mathrm{Re}(W_n W_{n-1} W_{n-2} - W_{n+1} W_n W_{n-1}) \rangle \ . \qquad (6)$$

If there is a net forward transport of enstrophy from the force to the enstrophy dissipation, the correlation functions (5) (and the analogous expressions for the other models) must be constant in the forward transport range. That gives the dimensional estimate

$$\langle |W_n| \rangle \ \sim \ \epsilon_\omega^{\frac{2}{3}} k_n^0, \qquad (7)$$

where ϵ_ω is the mean dissipation of enstrophy per unit time. Similarly in the inverse transport range one gets the estimate

$$\langle |W_n|^2 \rangle \ \sim \ \epsilon^{\frac{2}{3}} k_n^{\frac{4}{3}}, \qquad (8)$$

where ϵ is the mean dissipation of energy per unit time. The shell energy estimates are, respectively, $E_n \sim k_n^{-2}$ and $E_n \sim k_n^{-\frac{2}{3}}$, which is the same as the cascade estimates $E(k) \sim k^{-3}$ and $E(k) \sim k^{-\frac{5}{3}}$ for the full Navier-Stokes equations integrated over one octave in wave number space.

A. The GOY models in 2D

The GOY models are usually written in terms of complex shell velocities as

$$\frac{d}{dt}U_n = ik_n \Big(a_n U_{n+1}^* U_{n+2}^* + \frac{b_n}{2} U_{n-1}^* U_{n+1}^* + \frac{c_n}{4} U_{n-1}^* U_{n-2}^* \Big) - \nu k_n^2 U_n + f_n \ . \qquad (9)$$

We can transform (9) to (2) by absorbing a factor k_n in the shell variables. The particular form of the right-hand side of (9) ensures that the phase-space volume

$$dV = dU_1 \wedge dU_1^* \wedge \cdots \wedge dU_n \wedge dU_n^* \qquad (10)$$

is inertially conserved. The parameters values for which (9) conserve energy are given up to an overall factor by

$$a_n = 1, \quad b_n = -\epsilon, \quad c_n = -(1-\epsilon) \ . \qquad (11)$$

The bifurcations and transitions to chaos in (9) when changing ϵ have recently been investigated in [10]. If ϵ is greater than 1 there is a second conserved quantity $\sum k_n^{2\alpha} |U_n|^2$, the exponent α changing with ϵ [29].

Enstrophy conservation, i.e., $\alpha = 1$, is realized at the particular value ϵ equal to 1.25. The 2D GOY equations written for shell vorticity variables hence read

$$\frac{d}{dt}W_n = (W_{n+1}^* W_{n+2}^* - 5W_{n-1}^* W_{n+1}^* + 4W_{n-1}^* W_{n-2}^*) - \nu k_n^2 W_n - \nu' k_n^{-2\gamma} W_n + F_n \ . \qquad (12)$$

For convenience we have in (12) rescaled the W_n's to absorb an overall factor $\frac{i}{8}$ and added an artificial infrared viscosity.

In [16] a class of models was proposed which contain GOY-like interactions between triads of shells further apart. These models were further studied in the range of forward transport in [17]. For interactions decaying sufficiently fast with distance between interacting shells they behave quite similarly to the 2D GOY model.

B. The coupled GOY model

We motivate this model by the observation that the GOY models make no difference between velocity and vorticity, which only differ by a scale factor. It could therefore be hoped that a shell model which preserves some trace of the vector structure of the velocity field will be in a qualitative sense closer to the Navier-Stokes equations.

In 2D we can write the vorticity equation in Fourier space as

$$\frac{d}{dt}\hat{\omega}(\vec{k}) = \sum_{\vec{k}+\vec{k}'+\vec{k}''=0} \frac{\vec{k}' \times \vec{k}''}{|\vec{k}'|^2} \hat{\omega}(\vec{k}')\, \hat{\omega}(\vec{k}'') - \nu |\vec{k}|^2 \hat{\omega}(k) + F(k) \ . \qquad (13)$$

An obvious consequence of (13) is that two parallel vectors do not drive a third. We can model (13) by taking few shell variables $W_{n,j}$, $j = 0, 1, \ldots$, per shell, associate with each a wave vector $\vec{k}_{n,j}$ with length k_n and direction $\hat{e}_j$, and look for equations in the form

$$\frac{d}{dt}W_{n,j} = \sum_{\substack{n',j'\\ n'',j''}}^{\infty} C_{(n,j),(n',j'),(n'',j'')} \times \frac{\vec{k}_{n',j'} \times \vec{k}_{n'',j''}}{|\vec{k}_{n',j'}|^2} W^*_{n',j'} W^*_{n'',j''} - \nu k_n^2 W_{n,j} - \nu' k_n^{-2\gamma} W_{n,j} + F_{n,j} \quad (14)$$

with some interaction coefficients C chosen to preserve energy and enstrophy.

A simple implementation of (14) is to take wave vectors in a hexagonal pattern $\hat{e}_j = (\cos(2\pi j/3), \sin(2\pi j/3))$ for $j = 0, 1, 2$. One possible set of interactions is then the same as in the 2D GOY model, but going only between triples of shell variables having different directions:

$$\frac{d}{dt}W_{n,j} = (W^*_{n+1,j+1}W^*_{n+2,j+2} - 5W^*_{n+1,j+1}W^*_{n-1,j+2} + 4W^*_{n-2,j+1}W^*_{n-1,j+2}) + (W^*_{n+2,j+1}W^*_{n+1,j+2} - 5W^*_{n-1,j+1}W^*_{n+1,j+2} + 4W^*_{n-1,j+1}W^*_{n-2,j+2}) - \nu k_n^2 W_{n,j} - \nu' k_n^{-2\gamma} W_{n,j} + F_{n,j} \; . \quad (15)$$

In (15) we have used the notation that $W_{n,j+3} = W_{n,j}$. We will call (15) the coupled GOY model. It has some moderate numerical advantages over the original GOY model. Due to more variables per shell and more couplings, the coupled GOY model equilibrates faster. In the original GOY models with a steady force one observes that the shell energy spectrum in the inertial range exhibits oscillations superimposed on a mean power law. [9] We find no trace of such oscillations in (15) and conclude that three variables per shell is enough to sufficiently randomize the system and remove these undesired oscillations.

We have used forcing terms acting on shell 0 of the forms

$$F_{0,j} = \frac{\eta}{\sum_{j=0,1,2} |W_{0,j}|^2} W_{0,j} \; , \quad (16)$$

$$F_{0,j} = \frac{\eta}{\sum_{j=0,1,2} |W_{0,j}|^2} W^*_{0,j} \; . \quad (17)$$

The advantage of (16) and (17) is that the fluxes of energy and enstrophy from the force are fixed to be proportional to η, in the case of (16) exactly equal to η. For most of our simulations we have used the forcing (17) and artificial viscous terms such as $-\nu' k_n^{-2} W_{n,j}$, i.e., $\gamma = 1$.

III. THE STATISTICAL MECHANICS APPROACH

In the inviscid case the conservation laws and the Liouville theorem allows for an equilibrium statistical mechanics description. Here we review this approach due to Onsager [11], Hopf [12], and Lee [13]. For a later review see [14].

We consider the equations of two-dimensional hydrodynamics in Fourier space, with cutoffs $k_{\min}$ and $k_{\max}$. The lower cutoff can be realized physically by enclosing the system in a finite container. We need also the upper cutoff to avoid the ultraviolet catastrophe of classical continuous fields. As the system leaves inertially invariant the two quadratic forms energy and enstrophy, the canonical ensemble distribution function for the Fourier components of vorticity is

$$P(\hat{\omega}(\vec{k})) \propto \exp\{ -[\beta_1 |\hat{\omega}(\vec{k})|^2 + \beta_2 |\vec{k}|^{-2} |\hat{\omega}(\vec{k})|^2]/2 \} \; . \quad (18)$$

In (18) we have two Lagrange multipliers β_1 and β_2 or, alternatively, an "enstrophy temperature" T_1, equal to $1/\beta_1$, and an "energy temperature" T_2, equal to $1/\beta_2$. The second-order moment of (18) is

$$\langle |\hat{\omega}(\vec{k})|^2 \rangle = \frac{T_1}{1 + \frac{T_1}{T_2} |\vec{k}|^{-2}} \; , \quad (19)$$

which, depending on $|\vec{k}|^2$ and the temperatures, separates into two branches

$$\langle |\hat{\omega}(\vec{k})|^2 \rangle \sim \begin{cases} T_2 |\vec{k}|^2 & \text{if } |\vec{k}|^2 \ll \frac{T_1}{T_2} \\ T_1 & \text{if } |\vec{k}|^2 \gg \frac{T_1}{T_2} \end{cases} \; . \quad (20)$$

The energy spectra in these two ranges are $E(k) \sim k$ and $E(k) \sim k^{-1}$, respectively. As discussed above, at least the second prediction is clearly in disagreement with all numerical investigations of the 2D Navier-Stokes equations [18,28,19,26].

The argument for (18) translates immediately to the shell models considered in Sec. II. We then have the prediction that the shell variables are uncorrelated Gaussians with widths

$$\langle |W_n|^2 \rangle \sim \begin{cases} T_2 k_n^2 & \text{if } k_n^2 \ll \frac{T_1}{T_2} \\ T_1 & \text{if } k_n^2 \gg \frac{T_1}{T_2} \end{cases} \; . \quad (21)$$

The two branches in (21) simply correspond to shell energy equipartition and shell enstrophy equipartition. The shell energy prediction in the shell enstrophy equipartition branch is $E_n \sim k_n^{-2}$. We thus have that in 2D shell models, but not in 2D ideal hydrodynamics, the energy spectrum of one branch of a formal statistical equilibrium and of an assumed forward cascade of enstrophy exhibits the same scaling law.

We continue with some elementary considerations from nonequilibrium statistical mechanics [30]. Suppose that a physical system is not in thermal equlibrium, but the distribution functions at any point are close to the equilibrium distribution, with temperatures that change slowly in space. A heat flux is then set up, which acts to restore global equilibrium. In other words, the induced flux is

$$\vec{\Pi}_Q = -\kappa \vec{\nabla} T \; , \quad (22)$$

where the proportionality constant κ is the heat conduc-

tion coefficient, generally dependent on temperature.

We now translate this picture to the shell models. For definitiveness we consider the range of forward transport of enstrophy. The local "shell temperatures" of this nonequilibrium system are not defined *per se*, but may be specified by the expectation values

$$T_1(n) \quad = \quad \langle |W_n|^2 \rangle \ , \tag{23}$$

where the average is taken with respect to the the stationary distribution of the W_n's. In the first approximation, it is assumed that this joint distribution factorizes into uncorrelated Gaussians with widths $T_1(n)$. Then, if the shell temperatures of two nearest neighbor shells differ, we expect a flux of enstrophy through the nth shell

$$\Pi_n(\Omega) \ = \ -\kappa_1[T_1(n+1) - T_1(n)] \ , \tag{24}$$

where we can call the transport coefficient κ_1 the "shell enstrophy conductivity constant." In a steady state of forward flux of enstrophy, one thus has

$$T_1(n+1) = T_1(n) - \frac{\epsilon_\omega}{\kappa_1} \ , \tag{25}$$

where ϵ_ω is the mean dissipation of enstrophy per unit time.

The temperature dependence of κ_1 can be estimated as follows. The nonlinear inertial term in the shell model equations plays the role of the collision operator in kinetic theory. The transport coefficient is determined by the linearized collision operator. In the shell models the nonlinear terms are quadratic and hence the linearization is linear in the shell amplitudes. We therefore expect

$$\kappa_1 \sim \sigma\sqrt{T_1} \tag{26}$$

with some proportionality constant σ, as in the kinetic theory of gases.

When all the temperature increments are supposed small we have the prediction

$$T_1(n) \sim \left([T_1(n_f)]^{\frac{3}{2}} - \frac{3\epsilon_\omega}{2\sigma}(n - n_f) \right)^{\frac{2}{3}} \ , \tag{27}$$

where n_f is the shell of the forcing. At the dissipative end $T_1(n)$ eventually becomes much smaller than unity. We may therefore rewrite (27) as

$$T_1(n) \sim \left[\frac{3\epsilon_\omega}{2\sigma}(n_{\rm diss} - n) \right]^{\frac{2}{3}} \ , \qquad \nu k_{n_{\rm diss}}^2 \sim 1 \ . \tag{28}$$

We see that by coincidence the dependence on ϵ_ω is also as predicted by the cascade picture. The spectrum, however, depends logarithmically on ν through $n_{\rm diss}$. This contradicts the assumption of a cascade process independent of viscosity.

Finally, over small increments the transport coefficient are slowly varying and we have the shell model equivalent of Fourier's law of heat conduction:

$$T_1(n) \sim T_1(n_0) - \frac{\epsilon_\omega}{\kappa_1}(n - n_0) \ , \quad n - n_0 \ll n_{\rm diss} - n_f \ . \tag{29}$$

IV. NUMERICAL RESULTS ON THE STEADY STATE

In this section we present numerical results on the coupled GOY model (15). The first set of results, Figs. 1–6 is from one run of length 3×10^5 in time. Statistics was taken with a frequency of 1 Hz, about once per shell turnover time in the range of forward transport. By convention the force acted on shell zero. The viscosity was $\nu = 10^{-24}$. Practically all dissipation of enstrophy occurred in shells 34–42. The artificial viscous term was of the type $-\nu' k_n^{-2} W_n$ with $\nu' = 10^{-15}$. The energy output occurred in shells -21 to -14. We used the forcing of type (17) with η equal to one. The observed mean fluxes of enstrophy and energy were approximately 0.075. The

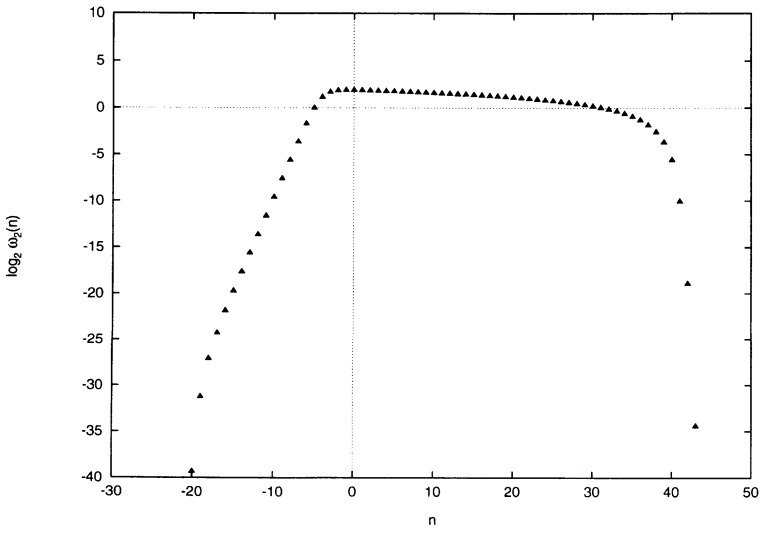

FIG. 1. The second-order structure function $\omega_2(n) = \langle \sum_j |W_{n,j}|^2 \rangle$ of shell vorticity as a function of shell number, on a logarithmic scale.

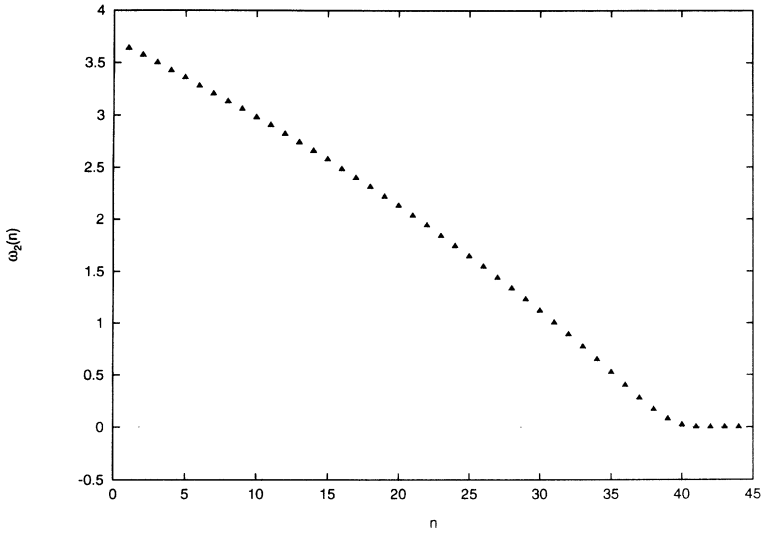

FIG. 2. The second-order structure function of vorticity as a function of shell number in the range of forward transport of enstrophy, on a real scale.

integration method was the slaved leapfrog scheme of [9] with a time step of 0.003.

Let us first look at Fig. 1, which shows the second moment of shell vorticity vs shell number. The dominant overall features are one branch at positive n's, which is nearly flat, i.e., implies $\langle |W_n|^2 \rangle \sim k_n^0$, and one branch at negative n's, which is closely fitted by $\langle |W_n|^2 \rangle \sim k_n^2$. Both results are in agreement with the predictions of a statistical equilibrium as in Sec. III. Let us add here that, according to Fig. 1, the characteristic times in the range of forward transport of enstrophy are about constant. This run therefore represents about 10^5 turnover times in all the forward range and there are indeed only small fluctuations. In contrast, in the inverse range the characteristic times are proportional to k_n^{-1}, which means that we have about one turnover time in the energy dissipation range. Looking closer at Fig. 1 we clearly see that the spectrum in the range of forward transport is not quite flat and that the "k_n^0 range" seems to extend about five shells to the left of the force. The second phenomenon is difficult to explain in the framework of the cascade picture. It is not a problem in the statistical equilibrium picture if we assume that the shell temperatures of enstrophy and energy are such that the bend in the curve occurs somewhat to the left of the force. The first phenomenon was observed in [17] and there attributed to a non-power-law correction on top of a power law with an exponent close to zero. Systematic investigations on the Yamada-Ohkitani models [31] gave only a preasymptotic correction and thus an asymptotic power law k_n^0. Figure 2 shows the second moments of the shell variables on a real scale instead of a logarithmic scale as in Fig. 1. A dominant linear trend is quite clear. The deviations from a pure power law in Fig. 1 are hence as predicted by (29) from the picture of weakly perturbed equilibria.

Figure 3 shows the numerically observed distributions in the forward range, compared with a Gaussian. The fit is clearly good. Figure 4 compares the numerically observed kurtosis of the shell enstrophies to the estimate

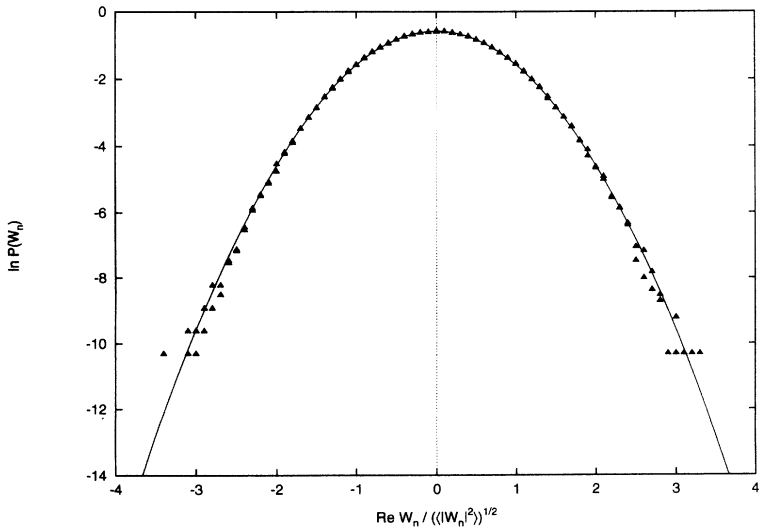

FIG. 3. Probability distribution function of the real parts of the shells variables $W_{5,0}$ and $W_{30,0}$ in the range of forward transport of enstrophy. The full line is a Gaussian distribution with the same variance.

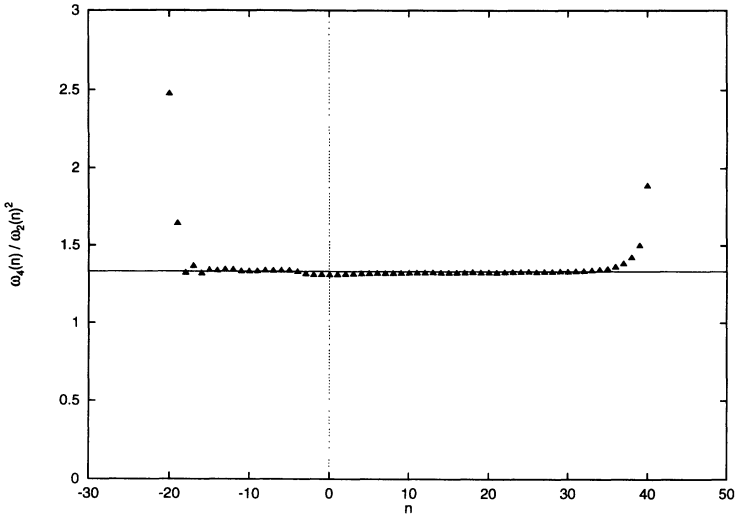

FIG. 4. The kurtosis $\omega_4(n)/\omega_2(n)^2$, where $\omega_4(n) = \langle(\sum_j |W_{n,j}|^2)^2\rangle$ of the shell vorticity distribution function. The horizontal line is the prediction if the three shell variables are assumed to be uncorrelated Gaussian variables with the same variance.

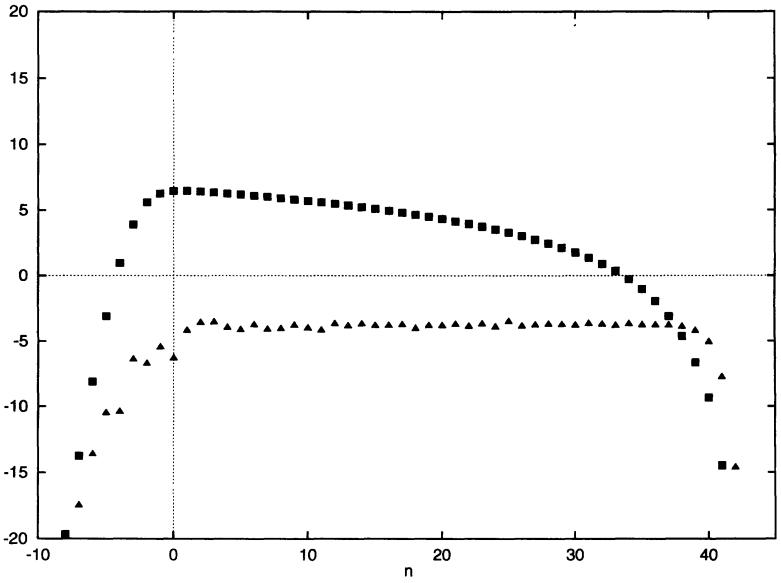

FIG. 5. The absolute value of mean enstrophy flux $\langle\Pi_n(\Omega)\rangle$ (triangle), and the mean squared enstrophy flux $\langle[\Pi_n(\Omega)]^2\rangle$ (square), on a logarithmic scale. At the peak the standard deviation of the flux is about 50 times larger than the mean value.

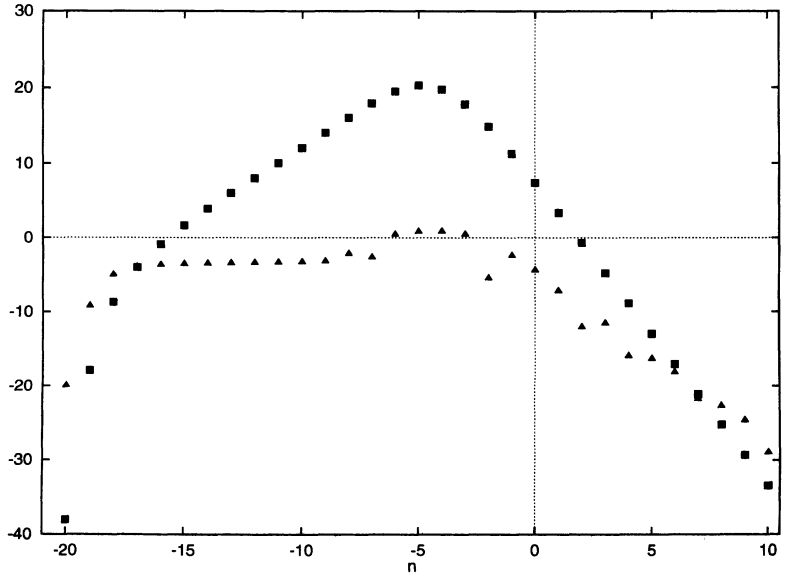

FIG. 6. The absolute value of mean energy flux $\langle\Pi_n(E)\rangle$ (triangle) and the mean squared energy flux $\langle[\Pi_n(E)]^2\rangle$ (square), on a logarithmic scale. At the peak the standard deviation of the flux is about 10 000 times larger than the mean value.

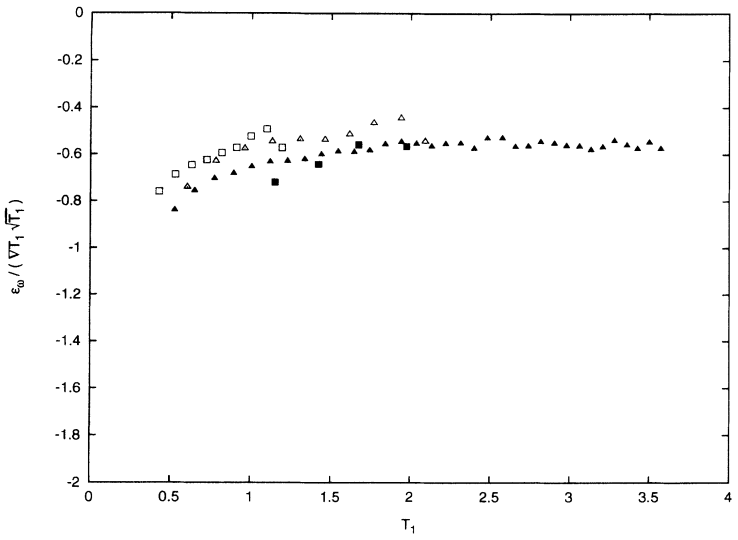

FIG. 7. Estimates of κ_1 for a system of 50 shells from -24 to $+25$. The symbols refer to runs with forcing (16) $\nu = 10^{-9}$, $\nu' = 10^{-6}$, and the flux is equal to 0.05 (open squares); $\nu = 10^{-9}$, $\nu' = 10^{-6}$ and flux is equal to 0.1 (open triangles); $\nu = 10^{-6}$, $\nu' = 10^{-4}$, and the flux is equal to 0.2 (solid squares). The solid triangles refer to the data of Fig. 2.

that the three variables in one shell are uncorrelated Gaussians with the same variance. Again the fit is quite good. This analysis in the inverse range leads to similar scenario. Taken together these results imply that to a good approximation there are no observable correlations between the shell variables within one shell. We have also checked directly that this is true. In addition there are no measurable correlations between shell variables in two nearest neighbor shells.

Figure 5 shows the mean enstrophy flux and the mean squared enstrophy flux. The curve of mean enstrophy flux should be flat and is so to a much better approximation than the second moment in Fig. 1.

Figure 5 shows that the standard deviation of the flux is about 50 times higher than the mean value in the beginning of the range of forward transport and then decreases, but stays above the mean flux up to the dissipative range. The mean flux shows a clear downward jump from shell 1 to shell 0, and then a fast decrease for negative n. In this range the eventual mean transport can only vanish and the nonzero values represent fluctuating incremented averages taken over finite time.

Figure 6 shows the mean energy flux and the mean squared energy flux. Toward the energy dissipation range the mean flux is to good approximation constant and agrees with the mean energy infused to the system per unit of time. At the top value around five shells to the left of the forcing, the standard deviation of the energy flux is about 10 000 times larger than the mean value. From the value of the variance of the flux, about 10^6, and the number of measurements 3×10^5, one sees that the rise of the curve of the energy flux below the top value of the flux squared curve is a statistical measurement error. We have checked that this explanation is correct by comparing with other runs with higher artificial viscosity for which the range of inverse energy transport is shorter and the times to reach an asymptotic state at the energy dissipation scale is shorter.

The second set of results is a direct test of Eq. (26), from different runs with different viscosities and different forward enstrophy flux. Figure 7 shows that κ_1 scales to a good approximation as $\sqrt{T_1}$, as expected by our theoretical arguments.

V. DYNAMICAL BEHAVIOR

In this section we briefly discuss the "instability properties" of the 2D shell models (15) by studying the behavior of the Lyapunov exponent λ as a function of the Reynolds number Re, the fluctuations of the effective Lyapunov exponent γ_τ, the tangent vector, and the spatial spreading of a small perturbation initially localized on a given shell.

Given a dynamical system described by a set of differential equations

$$\frac{dx}{dt} = F[x(t)] \,, \tag{30}$$

the response of the system to a perturbation $\delta x(t+\tau)$ of its state at time t after a delay τ is measured by the error growth rate

$$R_t(\tau) \equiv \frac{|z(t+\tau)|}{|z(t)|} \simeq \frac{|\delta x(t+\tau)|}{|\delta x(t)|} \,, \tag{31}$$

where z is the tangent vector obeying the evolution equation

$$\frac{dz_i}{dt} = \sum_j \frac{\partial F_i[x(t)]}{\partial x_j} z_j . \tag{32}$$

By definition the largest Lyapunov exponent is

$$\lambda = \lim_{\tau \to \infty} \frac{1}{\tau} \langle \ln R_t(\tau) \rangle \,, \tag{33}$$

where the angular brackets denote a time average along the trajectory. The Oseledec theorem [32] ensures that if the average is removed, then for almost all initial conditions one obtains the same value for λ.

The exponent λ gives a global characterization of the "instability" of the trajectory. Local information can be

obtained from the effective Lyapunov exponent $\gamma_\tau(t)$ defined as

$$\gamma_\tau(t) = \frac{1}{\tau} \ln R_t(\tau) \tag{34}$$

and from its fluctuations [33].

The scenario that emerges is completely different from that observed for the 3D GOY model studied in [6]. The main results for the 3D model are the following.

(i) the Lyapunov exponent λ increases with the Reynolds number

$$\lambda \sim \mathrm{Re}^\alpha \text{ with } \alpha \simeq 0.46 \ , \tag{35}$$

in good agreement with the prediction of the multifractal generalization [34] of a Ruelle argument. [35]

(ii) The effective Lyapunov exponent γ_τ exhibits strong fluctuations at increasing Re. Its variance μ scales like

$$\mu = \lim_{\tau\to\infty} \tau\langle(\gamma_\tau - \lambda)^2\rangle \sim \mathrm{Re}^\beta \text{ with } \beta \simeq 0.8 \tag{36}$$

so that the ratio μ/λ, which gives a quantitative measure of the intermittency level [33], diverges with the Reynolds number.

(iii) The tangent vector during the intermittent bursts (of energy and chaoticity) is strongly localized on the shells corresponding to the Kolmogorov scale, while in the laminar phase it spreads over the whole inertial range. In addition there is a strong correlation between the intermittent bursts of energy dissipation, large fluctuations of the effective Lyapunov exponent, and the localization of the tangent vector on the Kolmogorov length.

(iv) There is a backward cascade for the propagation of a perturbation from small scales to large scales in qualitative agreement with the phenomenological scenario proposed by Lorenz [36]

The 2D shell models present a completely different behavior. The numerical study of the models introduced in this paper reveals the following scenario.

(i) The Lyapunov exponent depends very weakly on the Reynolds number

$$\lambda \sim \ln \mathrm{Re} \ ; \tag{37}$$

see Fig. 8. It is worth noting that even in the framework of the Kraichnan-Batchelor theory, one has the same prediction for 2D Navier-Stokes equations, by assuming that the Lyapunov exponent is proportional to the smallest characteristic time of the system.

(ii) The effective Lyapunov exponent has small fluctuations and $\mu \ll \lambda$.

(iii) The tangent vector is concentrated at the scale of the forcing.

(iv) A small perturbation initially concentrated about a given shell does not propagate by an inverse cascade mechanism, but diffuses through the shells. In Fig. 9 we report the spreading of a perturbation initially located on a small number of shells. The quantity shown in the figure is defined as

$$\delta W_n = \left[\sum_{j=0,1,2} (W_{n,j} - W'_{n,j})^2\right]^{1/2} \ , \tag{38}$$

where at the initial time $W'_{n,j}$ differs from $W_{n,j}$ by a quantity δ on shells $n = n_1, \ldots, n_2$. In the case reported in Fig. 9 we used $n_1 = -6$, $n_2 = -5$, and $\delta = 10^{-10}$. However, the curves are rather insensitive to the initial location of the perturbation.

The above results provide clear evidence that the "instability" behavior in the 2D shell models is very different from those of 3D shell models. Let us remark that the dynamical features observed for Eq. (15) are rather close to a scenario expected in equlibrium statistical mechanics.

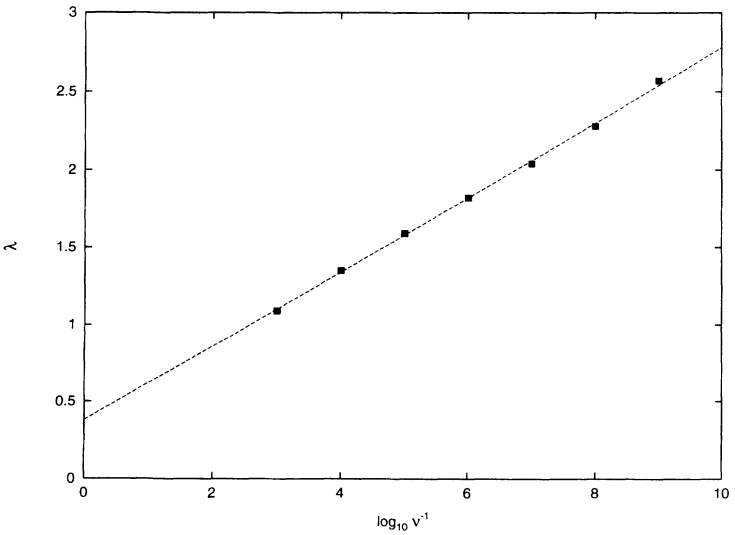

FIG. 8. Lyapunov exponent as a function of Reynolds number, defined as $\mathrm{Re} = \nu^{-1}$. The system consists of 50 shells from -24 to $+25$ with forcing (16) with $\eta = 0.1$ and $\nu' = 10^{-6}$.

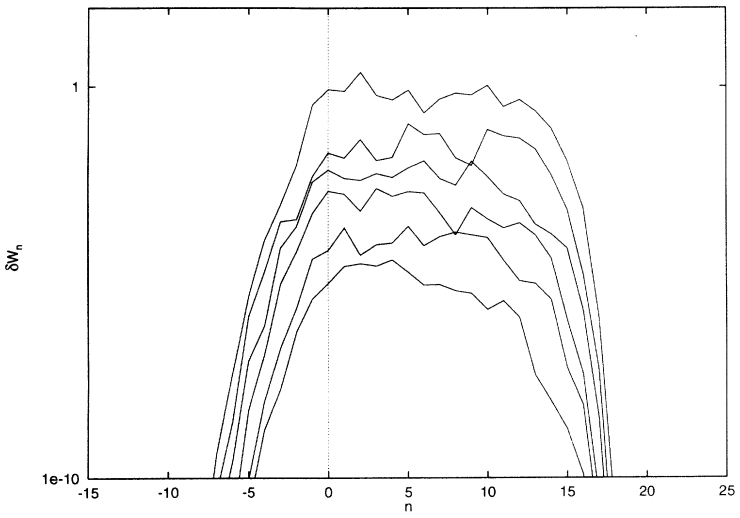

FIG. 9. Spreading of a perturbation as a function of time. The bottom curve refers to a time 0.2 s from the perturbation and the others, bottom to top, after time intervals of 0.4 s. The system consists of 50 shells from -24 to $+25$ with forcing (16) with $\eta = 0.1$, $\nu = 10^{-9}$, and $\nu' = 10^{-6}$. At the initial time the perturbation was of strength 10^{-10}. The curves are rather insensitive to the location of the initial perturbation; in the figure it is located on shells -6 and -5.

VI. DISCUSSION

We have presented numerical results of a wide class of shell models of 2D turbulence which can be simply and coherently explained by a formal nonequilibrium statistical mechanics, close to local equilibrium.

The weakly perturbed equilibrium predicts Gaussian probability distribution functions of the shell variables and the preasymptotic corrections to the power law in the forward range. Let us remark that these two observations are difficult to reconcile in a cascade picture where Gaussian probability distribution functions are possible if there is only one scaling exponent, "unifractality" [37]. However, in the absence of multifractality, it is hard to imagine mechanisms which are able to produce corrections to scaling such as pseudo algebraic power laws, the so-called multiscaling [38].

Finally, the mean values of the fluxes of both energy and enstrophy are always much smaller than the standard deviations. The fluxes are thus always small corrections superimposed on an mean randomly fluctuating state.

We therefore conclude that the models studied in this paper have very little to do with 2D turbulence.

A natural question at this point is the following: Why have shell models for 3D turbulence given reasonable results, while the 2D models have not? A qualitative answer goes as follows: The statistical equilibria picture should be relevant if the time scales of relaxation to local equilibrium are faster than the time scales of transport of the conserved quantities to the viscous sinks. The time scale for relaxation to local equilibrium can be estimated as the local shell turnover times, which in 3D shell models decrease with shell number (as $t_n \sim k_n^{-\frac{2}{3}}$ at the Kolmogorov fixed point). The time scale for transport to the energy dissipation range from a shell in the forward transport range can then be estimated as the geometric sum of the local turnover times up to the energy dissipation shell. Hence both time scales are of the same order and it is unlikely that 3D shell models display statistical equilibrium. Indeed a cascade scenario is observed.

On the contrary, in 2D shell models the local turnover times in the forward range are constant and the time to transport enstrophy to the dissipation range is proportional to how far away in shells that is. Therefore local statistical equilibrium has a chance to develop.

The question then arises of why this argument does not work for the 2D Navier-Stokes equations, where, in the Batchelor-Kraichnan cascade picture, the time scales in the forward range are also constant. One possible explanation is that one has to take into account the full nonlinearities of the Navier-Stokes equations with the nonlocal transfer of energy and enstrophy. A more interesting possibility is that the reason is that there are more states at high wave numbers and that the system gains entropy locally by transporting in that direction. It would then make sense to study simplified models, but where the number of states increases with shell number. Numerical experiments on one such model [39] lend support to this idea.

ACKNOWLEDGMENTS

This work was supported by the Swedish Natural Science Research Council under Contract No. S–FO 1778-302 (E.A.), by the French Government Program "Relance de l'Est" (P.F.), and by INFN (Iniziativa Specifica Meccanica Statistica FI3). E.A. thanks the Dipartimento di Fisica, Università di Roma "La Sapienza" for hospitality and financial support. G.B. thanks the Istituto di Cosmogeofisica del CNR, Torino, for hospitality. P. F. thanks the Laboratoire de Météorologie Dynamique, Ecole Normale Superieure, Paris, for hospitality.

[1] A.M. Obukhov, Atmos. Oceanic Phys. **7**, 41 (1971).
[2] V.N. Desnianskii and E.A. Novikov, J. Appl. Math. Mech. (USSR) **38**, 468 (1972).
[3] E.D. Siggia, Phys. Rev. A **15**, 1730 (1977).
[4] V.D. Zimin, Izv. Akad. Nauk SSSR, Fiz. Atmos. Okeana **17**, 941 (1981).
[5] M. Yamada and K. Ohkitani, J. Phys. Soc. Jpn. **56**, 4210 (1987); Phys. Rev. Lett. **60**, 983 (1988).
[6] M.H. Jensen, G. Paladin, and A. Vulpiani, Phys. Rev. A **43**, 798 (1991); **45**, 7214 (1992).
[7] J. Eggers and S. Grossmann, Phys. Lett. A **156**, 444 (1991).
[8] E.B. Gledzer, Dokl. Akad. Nauk SSSR **209**, 1046 (1973) [Sov. Phys. Dokl. **18**, 216 (1973)].
[9] D. Pisarenko, L. Biferale, D. Courvoisier, U. Frisch, and M. Vergassola, Phys. Fluid A **5**, 2533 (1993).
[10] L. Biferale, A. Lambert, R. Lima, and G. Paladin, Physica D (to be published).
[11] L. Onsager, Nuovo Cimento Suppl. **6**, 279 (1949).
[12] E. Hopf, J. Rat. Mech. Anal. **1**, 87 (1952).
[13] T.D. Lee, Q. Appl. Math. **10**, 69 (1952).
[14] R.H. Kraichnan and D. Montgomery, Rep. Prog. Phys. **43**, 547 (1980).
[15] M. Yamada and K. Ohkitani, Prog. Theor. Phys. **79**, 1265 (1988).
[16] P.G. Frick, Magnetohydrodynamics **19:1**, 48 (1983) (translated from Russian).
[17] P.G. Frick and E. Aurell, Europhys. Lett. **24**, 725 (1993).
[18] U. Frish and P. Sulem, Phys. Fluids **27**, 1921 (1984).
[19] V. Borue, Phys. Rev. Lett. **72**, 1475 (1994).
[20] A.N. Kolmogorov, C.R. Acad. Sci. USSR **30**, 301 (1941).
[21] G. Batchelor, Phys. Fluids Suppl. II **12**, 233 (1969).
[22] R.H. Kraichnan, Phys. of Fluids **10**, 1417 (1967).
[23] A. Monin and A. Yaglom, *Statistical Fluid Mechanics* (MIT Press, Cambridge, MA, 1971).
[24] F. Anselmet, Y. Gagne, E.J. Hopfinger, and R. Antonia, J. Fluid Mech. **140**, 63 (1984).
[25] B. Castaing, Y. Gagne, and E.J. Hopfinger, Physica D **46**, 177 (1990).
[26] C. Basdevant and Y. Couder, J. Fluid Mech. **173**, 225 (1986).
[27] R. Benzi, G. Paladin, G. Parisi, and A. Vulpiani, J. Phys. A **17**, 3521 (1984).
[28] M. Smith and V. Yakhot, Phys. Rev. Lett. **71**, 352 (1993).
[29] K. Ohkitani and M. Yamada, Prog. Theor. Phys. **81**, 329 (1989).
[30] L. Landau and E. Lifshitz, *Course on Theoretical Physics: Physical Kinetics* (Pergamon, New York, 1981), Vol. 10.
[31] G. Boffetta (unpublished).
[32] V.I. Oseledec, Trans. Moscow Math. Soc. **19**, 197 (1968).
[33] R. Benzi, G. Paladin, G. Parisi, and A. Vulpiani, J. Phys. A **18**, 2157 (1985).
[34] A. Crisanti, M.H. Jensen, G. Paladin, and A. Vulpiani, Phys. Rev. Lett. **70**, 166 (1993); J. Phys. A **26**, 6943 (1993).
[35] D. Ruelle, Commun. Math. Phys. **87**, 287 (1982).
[36] E. Lorenz, Tellus **21**, 3 (1967).
[37] R. Benzi, L. Biferale, G. Paladin, A. Vulpiani, and M. Vergassola, Phys. Rev. Lett. **67**, 2299 (1991).
[38] U. Frish and M. Vergassola, Europhys. Lett. **15**, 439 (1991).
[39] E. Aurell, P. Frick, and V. Shaidurov, Physica D **72**, 95 (1994).